Structural Engineering and Mechanics, *Vol. 57, No. 2 (2016) 221-238*
DOI: http://dx.doi.org/10.12989/sem.2016.57.2.221

Dynamic analysis of helicoidal bars with non-circular cross-sections via mixed FEM

Nihal Eratlı*, Murat Yılmaz[a], Kutlu Darılmaz[b] and Mehmet H. Omurtag[c]

Department of Civil Engineering, Istanbul Technical University, Istanbul, Turkey

(Received January 22, 2015, Revised December 7, 2015, Accepted December 8, 2015)

Abstract. One of the objectives of this study is to implement the direct calculation of the torsional moment of inertia for non-circular cross-sections, which is based on the St. Venant torsion formulation and the finite element method. Recently the proposed method provides a unique calculation of the torsional rigidity of simply and multiply connected cross-sections. Next, free vibration analyses of cylindrical and non-cylindrical helices with non-circular cross-sections are solved by a curved two-nodded mixed finite element based on the Timoshenko beam theory. Some thin-thick closed or open sections are handled and the natural frequencies of cylindrical and non-cylindrical helices are compared with the literature and the commercial finite element program SAP2000.

Keywords: mixed finite element; non-cylindrical helix; non-circular cross-sections; Poisson's equation; torsional moment of inertia

1. Introduction

Numerous theoretical and numerical studies for the static and the dynamic analysis of the cylindrical and non-cylindrical helices with the circular and the rectangular cross-sections are available in the literature. The governing differential equations developed by Michell (1890) go back to the 19th century and they were improved by Love (1899) and modified by Yoshimura and Murata (1952). The rotary inertia and the shear influence were included by Wittrick (1966) as a set of 12 linear coupled partial equations. An extensive historical review exists in Jiang *et al.* (1991), which provides a theoretical investigation of a coupled extensional-torsional vibration of helical springs. Lin and Pisano (1987) derived the general dynamic equations of helical springs. Analytical studies of Yu *et al*. (2010), Yu and Hao (2011) considered the warping deformations of the cross-section in a dynamic analysis of helicoidal springs and bars. Zhu *et al*. (2013) investigated the natural frequencies of a cylindrical helical spring using the Frobenius' scheme and the dynamic stiffness method. Since the natural frequencies of non-cylindrical helical springs depend on various parameters, such as the helix pitch angle, the helix geometry (hyperboloidal,

*Corresponding author, Associate Professor, E-mail: eratli@itu.edu.tr
[a]Ph.D., E-mail: yilmazmura@itu.edu.tr
[b]Professor, E-mail: darilmazk@itu.edu.tr
[c]Professor, E-mail: omurtagm@itu.edu.tr

http://www.techno-press.org/?journal=sem&subpage=8 ISSN: 1225-4568 (Print), 1598-6217 (Online)

barrel, and conical), the ratio of the maximum helix radius to the minimum helix radius, the geometry of the cross-section, the number of active turns, and the boundary conditions, obtaining analytical solutions in such an extensive range is challenging. To address these problems, various numerical methods were employed. Wittrick's equations were extended to numerical methods, e.g., applied to the finite element method (FEM) by Mottershead (1980) and the transfer matrix method by Pearson (1982). Nagaya *et al*. (1986) experimentally and theoretically determined the natural frequencies for non-cylindrical helical springs with circular cross-sections using the transfer matrix method. The transfer matrix method (TMM) is intensively applied to dynamic analysis of cylindrical/non-cylindrical helical springs besides FEM with circular and rectangular cross-sections by Yıldırım (1996), Yıldırım and İnce (1997), Yıldırım (1997), Yıldırım (1998) and Yıldırım (2002). Yıldırım (2012) derived linearized disturbance dynamic equations for buckling and the free vibration of cylindrical helical coil springs under combined compression and torsion. Based on Eisenberger (1990), Busool and Eisenberger (2002) employed the exact element method for the free vibration analysis of non-cylindrical helicoidal beams with circular and rectangular variable cross-sections. Omurtag and Aköz (1992) suggested a simple but effective formulation for solving non-cylindrical helix geometry, which considers the nodal curvature values of the nodes of the curved element; it was also verified by Girgin (2006). Lee (2007a, b) applied the pseudospectral method to investigate the free vibration analysis of cylindrical and non-cylindrical helical springs with circular cross-sections. Improved Riccati transfer matrix method is applied to non-cylindrical and composite non-cylindrical springs for analyzing the warping effect on the free vibration analysis by Yu and Hao (2012), Yu and Hao (2013a, b). Using the initial value method, free vibration analysis of circular beams, considering transverse shear deformation and rotary inertia, were investigated by Tufekci and Yigit (2012). Rajasekaran (2013) applied the differential quadrature element of lowest order or Lagrangian interpolation technique to solve the free vibration of functionally graded circular, parabolic, catenary, elliptic and sinusoidal arches. Fard (2014) investigated the eigenvalue governing equations based on Hamilton's principle using Fourier series solution method and by an adequate modeling of warping, shear correction factor was not required. A parametric study on the free vibration analysis of cylindrical and non-cylindrical helicoidal bars with thin-walled circular tube cross-section is performed by Eratlı *et al.* (2015).

Torsional rigidity of an arbitrary cross-section, with the exception of a circular cross-section, requires special care. Some analytical equations (e.g., Wang 1953, Timoshenko and Goodier 1969, Murray 1986) and approximated analytical formulas in tabulated form exist in Arutunan and Abraman (1963). The torsional stiffness of thin walled multi-celled structures, which are calculated using a membrane analogy and an arithmetic process of successive approximations, were tabulated by Roark (1954). Generally, analytical solutions for complicated arbitrary cross-sections are difficult to obtain. To overcome this problem, some numerical studies were developed. The boundary conditions of the well-known Poisson's equation and the St. Venant torsion formulation are deeply investigated in conjunction with the divergence theorem. The St. Venant torsion problem was solved by the finite difference method for a non-homogeneous and compound bar by Ely and Zienkiewicz (1960); the same theory was employed by Krahula and Lauterbach (1969) and solved the torsional stiffness and the shear stress for a hollow square section using the FEM. A boundary element solution was adapted to the St. Venant semi-inverse method to solve coupled torsion and flexure problems of arbitrary cross-sections and isotropic material by Friedman and Kosmatka (2000). The boundary element method was developed for the non-uniform torsion of arbitrary constant cross-sections of multi-material composite bars by

Sapountzakis (2001) and arbitrary variable cross-sections of simply or multiply connected bars by Sapountzakis and Mokos (2004). The most powerful approach was proposed by Prandtl, in which the torsion problem was reduced to the solution of Poisson's equation with a homogenous boundary condition (Timoshenko and Goodier 1969). Thus, the torsion problem yields to a standard two dimensional potential problem, which is suitable for a finite difference (Wang 1953) or FE solution (Hermann 1965, Darılmaz *et al.* 2007, Li *et al.* 2000). Lamancusa and Saravanos (1989) applied two dimensional thermal analogy and FEM for solving hollow square tubes.

In this study, the torsional moments of inertia for non-circular cross-sections are calculated by an alternative elegant FE solution of Poisson's equation, in contrast to the classical procedure. This program is embedded in a mixed FE program, which was developed based on the Timoshenko beam theory (Omurtag and Aköz 1992). First the torsional moment of inertia of simply and multiply connected cross-sections (hollow and composite) are calculated, and the results are verified with analytical and/or empirical formulas existing in the literature. Since multiply connected sections technically can be handled as a composite section, the proposed solution technique can be used to easily solve these sections. As a numerical investigation, a free vibration analysis of cylindrical, conical, barrel and hyperboloidal helices is performed via the mixed FEM. The first five natural frequencies of a cylindrical helix with an equilateral triangle cross-section are verified with the analytical study (Yu and Hao 2011). The results for the conical, barrel and hyperboloidal helices are compared with the results from the commercial computer program SAP2000. Barrel and hyperboloidal helices with thin/thick square box, open and cruciform cross-sections are solved, and all are benchmark examples for the literature.

2. Torsional rigidity of arbitrary cross-sections

2.1 Classical theory of torsion

In the range of classical theory of torsion of beams for isotropic materials, one can select the displacement field of a non-circular cross-section, which is depicted in Fig. 1, as $\mathbf{u}(u_1, u_2, u_3)$ where $u_1 = -\beta x_2 x_3, u_2 = \beta x_1 x_3, u_3 = \beta \phi(x_1, x_2)$ where u_i represents the section displacement vector components, β is the angle of twist per unit length, and $\phi(x_1, x_2)$ is the warping displacement function (Fung 1965). The state of stress in the cross-sectional domain Ω must satisfy the equations of equilibrium div$\boldsymbol{\sigma}$=0 and the following condition on the boundary Γ, $\boldsymbol{\sigma}\mathbf{n}$=0 where $\boldsymbol{\sigma}$ is the stress tensor, $\mathbf{n}$ is the unit normal vector and $\mathbf{t}$ is the corresponding tangent vector of the boundary (see Fig. 1). For a linear-elastic isotropic material, the stress tensor is expressed in $\phi_{,2}=\partial\phi/\partial x_2$ terms of the Lamé constants λ and μ and the small strain tensor $\mathbf{E}$ as

$$\boldsymbol{\sigma} = \lambda \mathrm{tr}(\mathbf{E})\mathbf{I} + 2\mu\mathbf{E} \quad \text{and} \quad \mathbf{E} = \tfrac{1}{2}\left(\nabla\mathbf{u} + (\nabla\mathbf{u})^{\mathrm{T}}\right) \tag{1}$$

where $\mu=G$ is the shear modulus. By inserting the displacement field $\mathbf{u}(u_1, u_2, u_3)$ into Eq. (1), the only non-zero stresses are determined to be

$$\sigma_{31} = \mu\beta(\phi_{,1} - x_2) \quad , \quad \sigma_{32} = \mu\beta(\phi_{,2} + x_1) \tag{2}$$

where the partial differentiation notation is $\phi_{,1}=\partial\phi/\partial x_1$ and. By introducing scalar field function Φ as

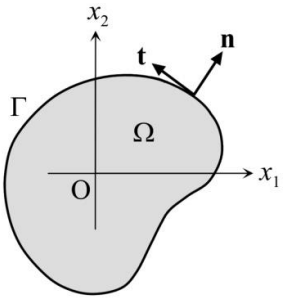

Fig. 1 Non-circular cross-section

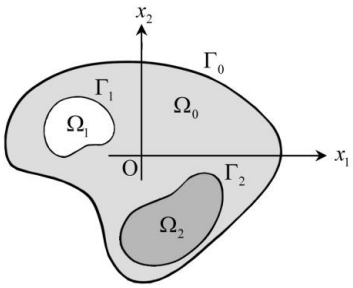

Fig. 2 Multiply connected region

$$\sigma_{31} = \mu\beta\Phi_{,2} \quad , \quad \sigma_{32} = -\mu\beta\Phi_{,1} \tag{3}$$

the equilibrium equations in div**σ**=**0** are identically satisfied (Smith 1996). Using the compatibility condition for the warping displacement field yields

$$\Phi_{,11} + \Phi_{,22} = -2 \tag{4}$$

which is the governing equation for the torsion problem (Poisson's equation). Recalling the boundary condition in **σn**=**0**, the following expression must hold at every point on Γ

$$\left(\sigma_{31} n_1 + \sigma_{32} n_2\right)\Big|_{\Gamma} = \mu\beta\left(\Phi_{,2} n_1 - \Phi_{,1} n_2\right)\Big|_{\Gamma} = 0 \tag{5}$$

where n_1 and n_2 are the direction cosines of the boundary vector **n**. Eq. (5) is valid for uncoupled torsion and denotes the tangential derivative of the scalar field. Thus, Φ is constant on the boundary Γ. The torsional constant I_3 of the cross-section, in terms of the scalar field, is expressed as

$$I_3 = -\int_{\Omega}\left(\Phi_{,1} x_1 + \Phi_{,2} x_2\right)\mathrm{d}\Omega \tag{6}$$

Defining a vector field Θ on Ω as $\Theta=\{\Phi x_1, \Phi x_2\}^T$ and using the divergence theorem yields

$$-\int_{\Omega}(\Phi_{,1}x_1 + \Phi_{,2}x_2)\mathrm{d}\Omega = 2\int_{\Omega}\Phi\mathrm{d}\Omega - \oint_{\Gamma}\Phi(x_1 n_1 + x_2 n_2)\mathrm{d}\Gamma \tag{7}$$

For the constant Φ, the boundary integral in Eq. (7) becomes

$$\oint_{\Gamma}\Phi(x_1 n_1 + x_2 n_2)\mathrm{d}\Gamma = 2\Phi A_{\Omega} \tag{8}$$

where A_Ω is the area of the domain Ω. Setting Φ=0 on Γ, the boundary term can be eliminated without loss of generality and the torsional constant; for simply connected regions, it can be calculated as

$$I_3 = 2\int_{\Omega}\Phi\,\mathrm{d}\Omega \tag{9}$$

Eq. (9) does not directly hold for multiply connected regions (Fig. 2), as can be concluded from Eq. (7), since the boundary term of Eq. (7) is not the one given with Eq. (5) and must be taken into account for the interior sub-domains. In this study, Eq. (6) is considered directly in order to calculate the torsional constant, which holds for both simply and multiply connected regions in the

same way as it does not include any boundary integral term. For the finite element analysis, the multiply connected region given in Fig. 2 must be completely meshed, including the internal sub-domains and only $\Phi=0$ on Γ_0 should be enforced for the boundary condition. The torsional stiffness of the entire section can be calculated by the contributions of the each individual region Ω_i as

$$\mu I_3 = -\sum_{i=0}^{N_s} \mu_i \int_{\Omega_i} \left(\Phi_{,1} x_1 + \Phi_{,2} x_2 \right) \mathrm{d}\Omega_i \tag{10}$$

where N_s is the number of sub-domains.

2.2 Finite element formulation of the torsion problem

To solve Eq. (4), we apply Galerkin's method. For any element domain Ω^e, the following equations must hold for a set of trial functions ψ_i

$$\int_{\Omega^e} \psi_i \left(\Phi^e_{,11} + \Phi^e_{,22} \right) \mathrm{d}\Omega^e = -2 \int_{\Omega^e} \psi_i \, \mathrm{d}\Omega^e \tag{11}$$

Defining a vector field $\boldsymbol{\Xi}$ on Ω^e as $\boldsymbol{\Xi} = \left\{ \psi_i \Phi^e_{,1}, \psi_i \Phi^e_{,2} \right\}^{\mathrm{T}}$ and using the divergence theorem, the weak form of Eq. (11) is obtained as

$$\int_{\Omega^e} (\psi_{i,1} \Phi^e_{,1} + \psi_{i,2} \Phi^e_{,2}) \mathrm{d}\Omega^e = 2 \int_{\Omega^e} \psi_i \mathrm{d}\Omega^e + \oint_{\Gamma^e} \psi_i \nabla \Phi^e \cdot \mathbf{n}^e \mathrm{d}\Gamma^e \tag{12}$$

The boundary terms in Eq. (12) cancel out during the assemblage of the FE equations for adjacent element edges in the cross-section domain Ω and they are also zero on the free edges (edges without an adjacent element) to satisfy the boundary condition of the torsion problem given by $\Phi=0$ on Γ_0. For the FE analysis the nine-node quadratic quadrilateral element was selected, as depicted in Fig. 3. The coordinate space interpolation is expressed as

$$\mathbf{x} = \left[\mathbf{X} \right] \boldsymbol{\psi} = \begin{bmatrix} x_{11} & x_{12} & \dots & x_{19} \\ x_{21} & x_{22} & \dots & x_{29} \end{bmatrix}_{2\times 9} \begin{Bmatrix} \psi_1 \\ \psi_2 \\ \vdots \\ \psi_9 \end{Bmatrix}_{9\times 1} \tag{13}$$

where the first and the second indices of x represents the Cartesian coordinate component and the node number, respectively. The trial function space Ξ, in terms of the dimensionless local coordinate system η_1, η_2 depicted in Fig. 3, are selected as

$$\Xi(\eta_1, \eta_2) = C_0 + C_1 \eta_1 + C_2 \eta_2 + C_3 \eta_1 \eta_2 + C_4 \eta_1^2 + C_5 \eta_2^2 + C_6 \eta_1^2 \eta_2 + C_7 \eta_1 \eta_2^2 + C_8 \eta_1^2 \eta_2^2 \tag{14}$$

where C_i are constants. The Jacobian matrix of the coordinate mapping is expressed as $[\mathbf{J}]=[\mathbf{X}][\partial\boldsymbol{\psi}]$ where the matrix $[\partial\boldsymbol{\psi}]$ is defined as follows

$$\left[\partial \boldsymbol{\psi} \right] = \begin{bmatrix} \partial\psi_1 / \partial\eta_1 & \partial\psi_1 / \partial\eta_2 \\ \partial\psi_2 / \partial\eta_1 & \partial\psi_2 / \partial\eta_2 \\ \vdots & \vdots \\ \partial\psi_9 / \partial\eta_1 & \partial\psi_9 / \partial\eta_2 \end{bmatrix} \tag{15}$$

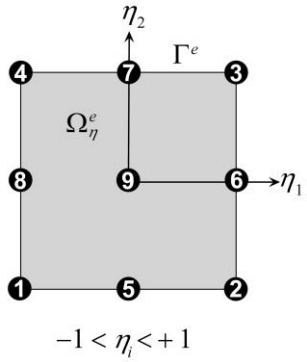

Fig. 3 Nine-nodded quadrilateral element

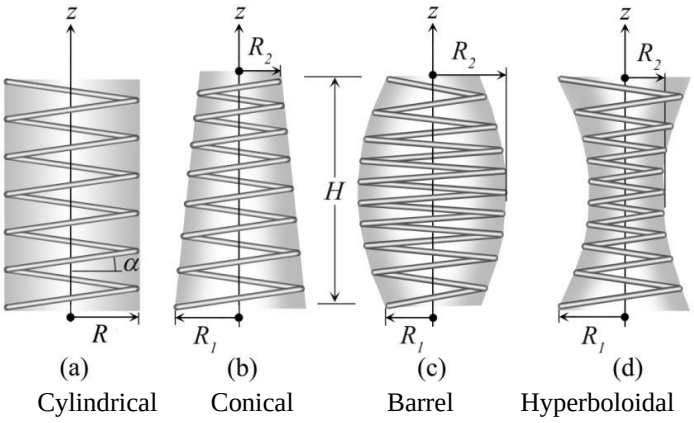

Fig. 4 Cylindrical and non-cylindrical helix geometries

In terms of the definitions, Eq. (12) can be written in matrix form as

$$\int_{\Omega_\eta^e} [\partial\boldsymbol{\psi}][\mathbf{J}]^{-1}[\mathbf{J}]^{-\mathrm{T}}[\partial\boldsymbol{\psi}]^{\mathrm{T}}\boldsymbol{\Phi}\left|\det[\mathbf{J}]\right| d\Omega_\eta^e = 2\int_{\Omega_\eta^e} \boldsymbol{\psi}\left|\det[\mathbf{J}]\right| d\Omega_\eta^e \tag{16}$$

where $\boldsymbol{\Phi}$ is the vector with the scalar field values at the element nodes as its components. Integrations are performed with the 3×3=9 point Gauss quadrature rule. By assembling Eq. (16) and solving the linear system of global equations, the values of the scalar field for the torsion problem can be obtained. The torsional constant in Eq. (6) can be calculated by considering the following contribution for each finite element as

$$\mu I_3 = -\sum_{e=1}^{N} \mu^e \int_{\Omega_\eta^e} \boldsymbol{\Phi}^{\mathrm{T}} [\partial\boldsymbol{\psi}][\mathbf{J}]^{-1}[\mathbf{X}]\boldsymbol{\psi}\left|\det[\mathbf{J}]\right| d\Omega_\eta^e \tag{17}$$

where N is the total number of elements.

3. The helix geometry and the functional

3.1 Helix geometry

The geometrical properties of the helices in Fig. 4 are $x=R(\varphi)\cos\varphi$, $y=R(\varphi)\sin\varphi$, $z=p(\varphi)\varphi$, $p(\varphi)=R(\varphi)\tan\alpha$, where α denotes the pitch angle, $R(\varphi)$ and $p(\varphi)$ signify the centerline radius and the step for unit angle, respectively, of the helix as a function of the horizontal angle φ. With $c(\varphi)=\sqrt{R^2(\varphi)+p^2(\varphi)}$, the infinitesimal arc length becomes $ds=c(\varphi)d\varphi$. In the cylindrical helix (see Fig. 4(a)), since $R=R(\varphi)$=constant and it is clear that $c=\sqrt{R^2+p^2}$, $\chi=R/c^2$, $\tau=p/c^2$, $p=R\tan\alpha$ are all constant. χ and τ are the curvature and torsion of the helix axis, respectively. The Frenet unit vectors are as follows: $\mathbf{t}$ is the tangent unit vector, $\mathbf{n}$ is the normal unit vector, $\mathbf{b}=\mathbf{t}\times\mathbf{n}$ is the binormal unit vector, and the differential relations between these unit vectors are expressed as $d\mathbf{t}/ds=\chi\mathbf{n}$, $d\mathbf{n}/ds=-\chi\mathbf{t}+\tau\mathbf{b}$ and $d\mathbf{b}/ds=-\tau\mathbf{n}$. In the case of a conical helix, the radius at any point on the helix geometry is $R(\varphi)=R_1+(R_2-R_1)(\varphi/2n\pi)$ where n is the number of active turns, R_1 and R_2 are the bottom radius and top radius, respectively, of the conical helix geometry (see Fig. 4(b)), and in the case of a barrel or hyperboloidal helix, the radius is $R(\varphi)=R_2+(R_1-R_2)(1-\varphi/n\pi)^2$ where R_1 and R_2 are the bottom radius and the central radius, respectively, of the barrel or hyperboloidal helix geometry (see Figs. 4(c)-(d)).

3.2 The functional

The field equations for the elastic helicoidal bar, which are based on the Timoshenko beam theory and refer to the Frenet coordinate system, are discussed in Omurtag and Aköz (1992) and Girgin (2006). Thus, the field equations can be written in the form

$$\left.\begin{aligned} -\mathbf{T}_{,s}-\mathbf{q}+\rho A\ddot{\mathbf{u}}=\mathbf{0} \\ -\mathbf{M}_{,s}-\mathbf{t}\times\mathbf{T}-\mathbf{m}+\rho\mathbf{I}\ddot{\boldsymbol{\Omega}}=\mathbf{0} \end{aligned}\right\} \tag{18}$$

$$\left.\begin{aligned} \mathbf{u}_{,s}+\mathbf{t}\times\boldsymbol{\Omega}-\mathbf{C}_\gamma\mathbf{T}=\mathbf{0} \\ \boldsymbol{\Omega}_{,s}-\mathbf{C}_\kappa\mathbf{M}=\mathbf{0} \end{aligned}\right\} \tag{19}$$

where, $\mathbf{u}(u_t, u_n, u_b)$ is the displacement vector, $\boldsymbol{\Omega}$ $(\Omega_t, \Omega_n, \Omega_b)$ is the rotational vector, $\ddot{\mathbf{u}}=\partial^2\mathbf{u}/\partial t^2$ and $\ddot{\boldsymbol{\Omega}}=\partial^2\boldsymbol{\Omega}/\partial t^2$ are the accelerations of the equation of motion, $\mathbf{T}(T_t, T_n, T_b)$ is the force vector, $\mathbf{M}(M_t, M_n, M_b)$ is the moment vector, $\mathbf{C}$ is the compliance matrix, ρ is the density of material, A is the area of the cross-section, $\mathbf{I}$ is the moment of inertia tensor, and $\mathbf{q}$ and $\mathbf{m}$ are the distributed external force vector and moment vector, respectively (Omurtag and Aköz 1992). Referring to the notation used for the moment of inertias given in Section 2 and the Frenet frame, note that $I_t=I_3$, $I_n=I_1$ and $I_b=I_2$. Eqs. (18)-(19) are written in operator form as $\mathbf{Q}=\mathbf{L}\mathbf{y}-\mathbf{f}$, after proving the operator to be potential and considering the harmonic motion of the helix in the free vibration analysis (and also $\mathbf{q}=\mathbf{m}=\mathbf{0}$), the functional yields to the following form (Oden and Reddy 1976, Omurtag and Aköz 1992)

$$\begin{aligned} \mathbf{I}(\mathbf{y}) = &-[\mathbf{u},\mathbf{T}_{,s}]+[\mathbf{t}\times\boldsymbol{\Omega},\mathbf{T}]-[\mathbf{M}_{,s},\boldsymbol{\Omega}]-\frac{1}{2}[\mathbf{C}_\kappa\mathbf{M},\mathbf{M}]-\frac{1}{2}[\mathbf{C}_\gamma\mathbf{T},\mathbf{T}]-\frac{1}{2}\rho A\omega^2[\mathbf{u},\mathbf{u}] \\ &-\frac{1}{2}\rho\omega^2[\mathbf{I}\boldsymbol{\Omega},\boldsymbol{\Omega}]+[(\mathbf{T}-\hat{\mathbf{T}}),\mathbf{u}]_\sigma+[(\mathbf{M}-\hat{\mathbf{M}}),\boldsymbol{\Omega}]_\sigma+[\hat{\mathbf{u}},\mathbf{T}]_\varepsilon+[\hat{\boldsymbol{\Omega}},\mathbf{M}]_\varepsilon \end{aligned} \tag{20}$$

where ω is the natural circular frequency and the square parentheses indicate the inner product. The terms with hats in Eq. (20) are known values on the boundary and the subscripts ε and σ represent the geometric and the dynamic boundary conditions, respectively.

4. The mixed finite element formulation

Using the subscripts i,j to represent the node numbers of the bar element, the linear shape functions $\phi_i=(\varphi_j-\varphi)/\Delta\varphi$ and $\phi_j=(\varphi-\varphi_i)/\Delta\varphi$ are employed in the FE formulation as stated by Omurtag and Aköz (1992), where $\Delta\varphi=(\varphi_j-\varphi_i)$. The non-cylindrical helix geometry is interpolated from the cylindrical geometry, using the $c^e=c_i\phi_i+c_j\phi_j$, $s^e=(c_i\phi_i+c_j\phi_j)\Delta\varphi$, $\chi^e=\chi_i\phi_i+\chi_j\phi_j$, $\tau^e=\tau_i\phi_i+\tau_j\phi_j$ where c_i, c_j are the exact nodal values of c^e, $s^e=c^e\Delta\varphi$ is the interpolated helix arc length for the element, χ_i, χ_j are the exact nodal curvatures and τ_i, τ_j are the exact nodal torsions of the helix geometry at nodes i, j, respectively. The curvatures are satisfied exactly at the nodal points and linearly interpolated through the element (Eratlı *et al.* 2014). The explicit form of the mixed FE matrices and sub-matrices exist in (Omurtag and Aköz 1992, Girgin 2006).

The problem of determining the natural frequencies of a structural system reduces to the solution of a standard eigenvalue problem $([\mathbf{K}]-\omega^2[\mathbf{M}])\{\mathbf{u}\}=\{\mathbf{0}\}$ where $[\mathbf{K}]$ is the system matrix, $[\mathbf{M}]$ is the mass matrix for the entire domain, $\mathbf{u}$ is the eigenvector (mode shape) and ω is the natural angular frequency of the system. Hence the explicit form of standard eigenvalue problem in the mixed formulation is

$$\left(\begin{bmatrix}[\mathbf{K}_{11}] & \mathbf{K}_{12}\\ \mathbf{K}_{21} & \mathbf{K}_{22}\end{bmatrix}-\omega^2\begin{bmatrix}[\mathbf{0}] & [\mathbf{0}]\\ [\mathbf{0}] & [\mathbf{M}]\end{bmatrix}\right)\begin{Bmatrix}\{\mathbf{F}\}\\ \{\mathbf{U}\}\end{Bmatrix}=\begin{Bmatrix}\{\mathbf{0}\}\\ \{\mathbf{0}\}\end{Bmatrix} \tag{21}$$

where $\{\mathbf{F}\}$ denotes the nodal force and the moment vectors and $\{\mathbf{U}\}=\{\mathbf{u}\ \boldsymbol{\Omega}\}^T$ signifies the nodal displacement and rotation vectors. To attain consistency between Eq. (21) and $([\mathbf{K}]-\omega^2[\mathbf{M}])\{\mathbf{u}\}=\{\mathbf{0}\}$, the $\{\mathbf{F}\}$ vector is eliminated in Eq. (21), which yields to the condensed system matrix $[\mathbf{K}^*]=[\mathbf{K_{22}}]-[\mathbf{K_{12}}]^T[\mathbf{K_{11}}]^{-1}[\mathbf{K_{12}}]$. Finally, the eigenvalue problem in the mixed formulation becomes $([\mathbf{K}^*]-\omega^2[\mathbf{M}])\{\mathbf{U}\}=\{\mathbf{0}\}$.

5. Numerical examples

5.1 Isotropic arbitrary cross-sections

The FE solutions of the torsional moment of inertia of the cross-sections given in Figs. 5(a)-(e) are verified with the literature (see Tables 1-6). A non-dimensional torsional inertia parameter $\bar{I}_t = I_t/a^4$ is employed for the sections. The convergence test for the square cross-section (see Fig. 5(a)) and the comparison with the literature (Wang 1953, Timoshenko and Goodier 1969, Krahula and Lauterbach 1969) exist in Table 1. For 225 numbers of unknowns, the percent difference with respect to the exact result (Timoshenko and Goodier 1969) is 0.04%. The results for the equilateral triangle cross-section (see Fig. 5(b)) are compared with Timoshenko and Goodier (1969), Friedman and Kosmatka (2000) in Table 2 and mesh refinement corresponding to 25 and 121 number of unknowns are given in Fig. 6. The distributions of element-wise contributions of Eqs. (9) and (10) of the equilateral triangular area are given in Fig. 7. For homogeneous medium both equations produce the same result with different distributions. As a multiply connected section example, a square box section (see Fig. 5(c)) with four different thickness-to-side ratios $\xi=t/a$ (0.040, 0.125, 0.250, 0.375) is employed and the convergence ability of the existing FE formulation is evident in Table 3. These results are compared with the formulas given by Murray (1986), Arutunan and Abraman (1963), Roark (1954), Krahula and Lauterbach (1969), Lamancusa

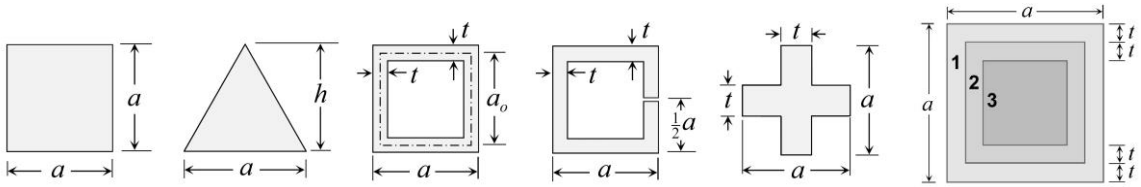

(a) square (b) equilateral triangle (c) square box (d) open square box (e) cruciform (f) composite square (t=0.04a)

Fig. 5 The cross-sections used in Examples 5.1 and 5.2

Table 1 $\bar{I}_t$ for the square cross-section

n_u	This study	Diff. %	n_e	FEM Krahula and Lauterbach (1969)	n_e	FD Wang (1953)	Exact Timoshenko and Goodier (1969)
1	0.13889	1.24					
9	0.13960	0.73					
49	0.14047	0.11	1024	0.14066	64	0.13859	0.14063
225	0.14057	0.04					
961	0.14058	0.04					

FEM: finite element method, FD: finite difference, n_u: number of unknowns, n_e:number of elements, Diff. % = (Timoshenko and Goodier (1969)-This study)×100/Timoshenko and Goodier (1969).

(a) n_u=25 (b) n_u=121

Fig. 6 Finite element mesh refinement of the equilateral triangular area by nine nodded elements
n_u: unmber of unknowns

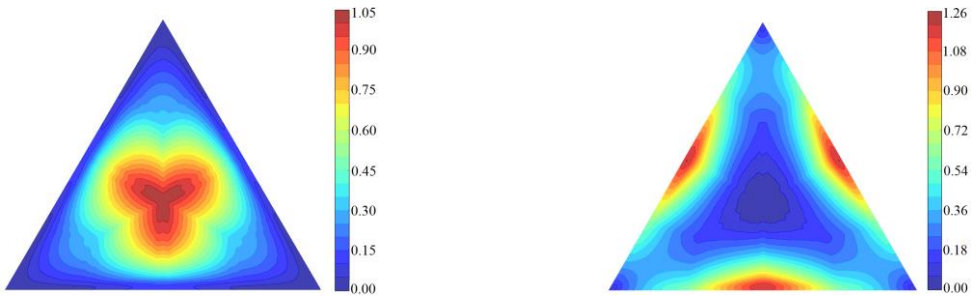

(a) (b)

Fig. 7 Distribution of element-wise contributions of Eqs. (9) and (10) depicted in contour plots (a) and (b) respectively. Section coordinate system is chosen as centroidal axes

Table 2 $\bar{I}_t$ for the equilateral triangle cross-section. Mesh refinement is given in Fig. 6

n_u	This study	Diff. %	n_e	BEM Friedman and Kosmatka (2000)	Exact Timoshenko and Goodier (1969)
25	0.021620	0.14			
121	0.021648	0.00	36	0.02165	0.02165
529	0.021650	0.00			

BEM: boundary element method, n_u: number of unknowns, n_e:number of elements,
Diff. % = (Timoshenko and Goodier (1969)-This study)×100/Timoshenko and Goodier (1969).

Table 3 $\bar{I}_t$ for the thin-thick close square box section

ξ=0.04		ξ=0.125		ξ=0.25		ξ=0.375	
n_u	This study	n_u	This study	n_u	This study	n_u	This study
17	0.036517	17	0.091982	17	0.130137	17	0.138526
73	0.036559	73	0.092114	73	0.130436	73	0.139758
305	0.036603	305	0.092235	305	0.130530	305	0.139912
1249	0.036618	1249	0.092251	1249	0.130540	1249	0.139929

(ξ=*t/a*, n_u: number of unknowns)

Table 4 $\bar{I}_t$ for the thin-thick square box section and the comparison with different approaches

	$\bar{I}_t$	ξ=*t/a*				
		0.04	0.125	0.25	0.375	0.5
Murray (1986)	$4/\oint \frac{ds}{t}$	0.0417	0.1429	0.3333	0.6000	1.0000
Roark (1954)	$\xi(1-\xi)^3$	0.0354	0.0837	0.1055	0.0916	0.0625
Arutunan and Abraman (1963)	$\xi - 2.5408\xi^2 + 2.644\xi^3 - 0.8344\xi^4$ where $\xi \leq 1/3$	0.0361	0.0903	0.1293	-	-
Krahula and Lauterbach (1969)	FEM ($n_e = 200$)	-	-	0.1293	-	-
Lamancusa and Saravanos (1989)	FEM	0.0373	0.0899	0.1287	-	0.1402
	$0.008 + 0.724\xi - 0.936\xi^2$	0.0355	0.0839	0.1305	0.1479	0.1360
	$0.978\xi - 2.309\xi^2 + 1.826\xi^3$	0.0355	0.0897	0.1287	0.1383	0.1400
	$\xi - 2.550\xi^2 + 2.670\xi^3 - 0.894\xi^4$	0.0361	0.0902	0.1289	0.1395	0.1404
This study	FEM	0.0366	0.0923	0.1305	0.1399	0.1406

and Saravanos (1989) in Table 4. The formulas given by Murray (1986) and Roark (1954) are appropriate for thin sections and Arutunan and Abraman (1963) is appropriate for $\xi \leq 1/3 \cong 0.333$. Note that the results for ξ =0.5 in Table 4 correspond to a solid square. As a simple section example, an open box section (see Fig. 5(d)) is solved using the following thickness-to-side ratios: ξ=*t/a* (0.040, 0.125, 0.250, 0.375). Convergence of the FE solution and the comparison of the final results for the ξ=*t/a*=0.040, 0.125 ratios with Arutunan and Abraman (1963) are displayed in Table 5. The formula given by Arutunan and Abraman (1963) is valid for $\xi \leq 1/6 \cong 0.1667$. For

Table 5 $\bar{I}_t$ for the thin-thick open square box type cross-section

ξ=0.04			ξ=0.125			ξ=0.25		ξ=0.375	
n_u	This study $\times 10^{-5}$	Arutunan and Abraman (1963) $\times 10^{-5}$	n_u	This study $\times 10^{-5}$	Arutunan and Abraman (1963) $\times 10^{-5}$	n_u	This study $\times 10^{-5}$	n_u	This Study $\times 10^{-5}$
171	8.153		113	226.442		85	1556.457	123	4420.374
965	8.199	8.192	313	228.994	227.865	149	1579.319	213	4432.007
4425	8.207		1457	229.506		735	1585.108	765	4448.146
-	-	-	3619	229.595		2645	1589.225	3817	4455.549

($\xi=t/a$, n_u: number of unknowns)

Table 6 $\bar{I}_t$ of the cruciform cross-section

$\xi=t/a$=1/5				$\xi=t/a$=1/3			
n_u	This study	Arutunan and Abraman (1963)	Sapountzakis and Mokos (2004)	n_u	This study	Arutunan and Abraman (1963)	Sapountzakis and Mokos (2004)
9	0.004852			9	0.022152		
57	0.005096			57	0.022670		
273	0.005161	0.00509	0.00520	273	0.022957	0.02279	0.02316
1185	0.005182			1185	0.023067		
4929	0.005189			4929	0.023110		
20097	0.005192			20097	0.023127		

(n_u: number of unknowns)

Table 7 Convergence of $\bar{I}_t$ $G/G_1=(\bar{I}_1 + 2\bar{I}_2 + 5\bar{I}_3)$ results for the composite square cross-section given in Fig. 5(f)

n_u	This study	Diff. %	SSD	ANSYS
33	0.465517	-0.78	0.45280	0.46913
137	0.466205	-0.63		
561	0.467013	-0.45		
2273	0.467044	-0.45		

(SSD: SAP2000 Section Designer, ANSYS: 3D Elasticity Brick Element (SOLID-186),
Diff. % = (This study-ANSYS)×100/This study)

cruciform cross-sections with ξ=1/5 and 1/3 ratios (see Fig. 5(e)), the torsional moment of inertia results are compared with Arutunan and Abraman (1963), Sapountzakis and Mokos (2004) in Table 6.

5.2 Composite square cross-section

A composite square cross-section with three different materials, as shown in Fig. 5(f), is selected where t=0.04a. The shear modulus of the sub-domains are G_2=2G_1 and G_3=5G_1, where G_1

Table 8 The comparison for the first five natural frequencies (Hz) of cylindrical helix with the equilateral triangle cross-section

Modes	This study	Diff.$^{(a)}$%	Diff. $^{(b)}$%	Yu and Hao (2011)		
				ANSYS $^{(a)}$	no warping	warped$^{(b)}$
1	193.4	-0.57	2.53	194.5	218.3	188.5
2	198.5	-0.10	1.26	198.7	219.9	196.0
3	204.7	-0.78	-0.29	206.3	260.5	205.3
4	296.1	0.74	0.78	293.9	294.0	293.8
5	397.8	-0.93	1.23	401.5	480.9	392.9

(Diff.$^{(i)}$ % = (This study-(Yu and Hao 2011))$^{(i)}$)×100/This study, i=a,b)

Table 9 The first nine natural frequencies (Hz) of conical helix with the square cross-section

Modes	This study (see Table 1 for I_t)						SAP2000				
	n_e	30	50	100	200	Diff.%	50	100	200	500	1000
1		386.10	393.32	393.39	393.40	-0.08	430.57	402.58	395.86	394.02	393.73
2		403.83	449.29	450.56	450.63	-0.14	467.86	455.29	452.25	451.44	451.28
3		419.95	501.51	509.94	510.43	-0.06	539.68	517.55	512.30	510.94	510.73
4		468.59	517.32	524.82	525.24	-0.09	552.46	532.00	527.15	525.89	525.70
5		714.14	744.24	744.96	744.98	-0.10	811.78	761.76	749.56	746.24	745.71
6		736.65	815.25	820.86	821.20	-0.23	868.16	833.96	825.75	823.46	823.06
7		759.99	852.00	860.67	861.15	-0.28	913.40	875.83	866.55	863.99	863.54
8		842.03	938.11	940.19	940.29	-0.22	983.21	952.25	944.82	942.78	942.38
9		878.85	1016.38	1018.64	1018.75	-0.13	1101.00	1039.70	1024.80	1020.80	1020.10

(R_2/R_1=0.5, Diff. % = (This study-SAP2000)×100/This study, n_e:number of elements)

is the shear modulus of the outermost layer. Table 7 shows the comparison of the torsional rigidity between the existing formulation and the commercial program results of the SAP2000 Section Designer and ANSYS. To obtain the correct results from the ANSYS elasticity FE solution, we considered the displacement readings from the midsection of a unit length composite bar defined by a total of 15249 SOLID-186 elements. Table 7 reveals that the formulation yields satisfying results.

5.3 The cylindrical helix with the equilateral triangle cross-section

The cylindrical helix fixed at both ends has an equilateral triangle cross-section (a=0.693 mm, see Fig. 5(b)) with the modulus of elasticity E=206 GPa, Poisson's ratio υ=0.3, the material density ρ=79000 kg/m^3, the number of active turns n=7.6, the pitch angle α=8.5744°, and the radius R=5 mm. The first five natural frequencies are calculated using 200 FEs, and the results are compared with Yu and Hao (2011) in Table 8. The warping included analytical result of Yu and Hao (2011) is quite in an agreement with the present mixed FE solution.

5.4 The conical helix with a square cross-section

In this section a dynamic analysis of a conical helix with a square cross-section (see Fig. 5(a))

that is fixed at both ends is considered. The material and geometrical properties are as follows: the modulus of elasticity E=210 GPa, Poisson's ratio υ=0.3, the material density ρ=7850 kg/m^3, the number of active turns n=6.5, the pitch angle α=4.8°, the bottom plane radius R_1=13 mm for the taper ratio R_2/R_1=0.5, and the dimension of the square cross-section of the helix a=2.6 mm. In Table 9, the mixed FE solutions for the first nine natural frequencies are compared using the commercial program SAP2000. The percent difference between these FE models is extremely small in the case of 1000 elements by SAP2000 and 200 elements by the present consistent mass mixed model.

5.5 Barrel helix with thin-thick and open-closed box cross-sections

The material and geometric properties of the barrel helix (see Fig. 4(c)) are as follows: the modulus of elasticity E=210 GPa, Poisson's ratio υ=0.3, the material density ρ=7850 kg/m^3, the number of active turns n=6.5, the pitch angle α=4.8° and the helix central-to-bottom radii ratio R_2/R_1=2.0 (assuming R_2=13 mm=constant). Two different boundary conditions are utilized, namely, fixed-fixed and fixed-free. Closed and open sections (see Figs. 5(c)-(d)) that range from thin to thick with four different thickness-to-side ratios $\xi=t/a$ (0.040, 0.125, 0.250, 0.375) where a=2 mm=constant are considered.

Thin-thick square box cross-section: Referring to the four different ξ ratios, the computed non-dimensional torsional inertia parameters are $\bar{I}_t = 0.0366$, 0.0923, 0.1305 and 0.1399 (see Table 4). The first six natural frequency results are compared using SAP2000 (via Section Designer) in Table 10. In the case of the fixed-fixed boundary condition, with respect to the fundamental

Table 10 The natural frequencies (Hz) of barrel type helix with the thin-thick square box sections and different boundary conditions

Modes	fixed-fixed											
	This study (n_e=200)				SAP2000 (n_e=1000)							
	$\xi=t/a$				$\xi=t/a$							
	0.04	0.125	0.25	0.375	0.04	Dif.%	0.125	Dif.%	0.25	Dif.%	0.375	Dif.%
1	335.1	314.9	286.2	265.3	334.4	0.21	313.7	0.38	286.6	-0.14	266.6	-0.49
2	365.3	336.5	301.5	278.2	366.4	-0.30	337.4	-0.27	302.4	-0.30	279.1	-0.32
3	446.6	414.5	373.4	345.3	446.8	-0.04	414.4	0.02	374.0	-0.16	346.3	-0.29
4	446.8	414.6	373.4	345.3	446.8	0.00	414.4	0.05	374.1	-0.19	346.4	-0.32
5	621.0	584.1	531.3	492.7	619.8	0.19	581.5	0.45	531.9	-0.11	495.2	-0.51
6	716.8	664.5	598.0	552.8	720.1	-0.46	667.0	-0.38	601.1	-0.52	556.0	-0.58
	fixed-free											
1	101.2	94.3	85.1	78.7	100.9	0.30	93.8	0.53	85.0	0.12	78.8	-0.13
2	101.7	94.7	85.5	79.0	101.4	0.29	94.3	0.42	85.3	0.23	79.1	-0.13
3	153.3	144.3	131.3	121.8	152.9	0.26	143.5	0.55	131.3	0.00	122.3	-0.41
4	199.6	183.7	164.4	151.5	200.4	-0.40	184.4	-0.38	165.0	-0.36	152.1	-0.40
5	397.6	369.4	333.0	307.9	398.4	-0.20	369.8	-0.11	334.0	-0.30	309.3	-0.45
6	398.8	370.7	334.2	309.1	399.7	-0.23	371.0	-0.08	335.3	-0.33	310.5	-0.45

(a=2 mm, R_2=13 mm, R_2/R_1=2.0, Diff. % = (This study-SAP2000)×100/This study)

Table 11 The natural frequencies (Hz) of barrel type helix with the thin-thick open square box sections and different boundary conditions

Modes	fixed-fixed											
	This study (n_e=200)				SAP2000 (n_e=1000)							
	ξ=t/a				ξ=t/a							
	0.04	0.125	0.25	0.375	0.04	Dif.%	0.125	Dif.%	0.25	Dif.%	0.375	Dif.%
1	16.1	50.5	101.4	151.5	16.2	-0.62	50.7	-0.40	101.4	0.00	151.8	-0.20
2	31.0	93.5	185.7	258.4	31.0	0.00	93.8	-0.32	185.8	-0.05	259.1	-0.27
3	33.5	103.7	197.2	261.1	33.8	-0.90	104.3	-0.58	196.4	0.41	260.8	0.11
4	34.0	105.0	197.4	277.2	34.0	0.00	104.8	0.19	197.8	-0.20	278.0	-0.29
5	42.1	131.9	263.1	283.1	-	-	-	-	-	-	283.7	-0.21
6	42.4	132.4	263.8	387.8	42.3	0.24	132.4	0.00	263.9	-0.04	-	-
	fixed-free											
1	6.3	19.7	38.1	53.3	6.3	0.00	19.7	0.00	38.0	0.26	53.2	0.19
2	6.5	20.2	38.9	54.2	6.5	0.00	20.2	0.00	38.8	0.26	54.1	0.18
3	7.3	23.0	46.1	69.0	7.4	-1.37	23.0	0.00	46.1	0.00	69.0	0.00
4	20.9	65.6	131.7	151.4	-	-	-	-	-	-	151.9	-0.33
5	21.9	68.7	137.7	196.5	22.0	-0.46	69.0	-0.44	137.7	0.00	-	-
6	28.2	87.3	163.9	206.5	28.3	-0.35	87.6	-0.34	164.2	-0.18	206.9	-0.19

(a=2 mm, R_2=13 mm, R_2/R_1=2.0, Diff. % = (This study-SAP2000)×100/This study)

natural frequency for the ξ=0.04 ratio, the reductions for the next three ξ ratios are 6.0%, 14.6% and 20.8%. Similarly, in the case of the fixed-free boundary condition, with respect to the fundamental natural frequency for the ξ=0.04 ratio, the reductions for the next three ξ ratios are 6.8%, 15.9% and 22.2%.

Thin-thick open square box type cross-section: Referring to the four different ξ ratios, the computed non-dimensional torsional inertia parameters are $\bar{I}_t = 8.2\times10^{-5}$, 22.96×10^{-5}, 1589.2×10^{-5} and 4455.5×10^{-5} (see Table 5). The first six natural frequencies are compared using SAP2000 (via Section Designer) in Table 11. In the case of the fixed-fixed boundary condition, with respect to the fundamental natural frequency for the ξ=0.04 ratio, the increases for the next three ξ ratios are 211.7%, 525.9% and 841.0%. Similarly, in the case of the fixed-free boundary condition, with respect to the fundamental natural frequency for the ξ=0.04 ratio, the increases for the next three ξ ratios are 212.7%, 504.8% and 746.0%.

For the fundamental natural frequencies of the fixed-fixed boundary condition, the results of the square box section for each ξ ratio are decreased by 95.2%, 84.0%, 64.6%, and 43.0% with respect to the open square box type cross-section results. In the case of the fixed-free boundary conditions, the results of the closed square box section for each ξ ratio are decreased by 93.8%, 79.1%, 55.2%, and 32.3% with respect to the open square box cross-section results.

5.6 Hyperboloidal helix with cruciform cross-section

The material and geometrical properties of the hyperboloidal helix (see Fig. 4(d)) are identical to the barrel helix, which was solved in Section 5.5. The helix central-to-bottom radii ratio

Table 12 The natural frequencies (Hz) of hyperboloidal type helix with the cruciform cross-section and different boundary conditions

Modes	fixed-fixed						fixed-free					
	This study (n_e=200)		SAP2000 (n_e=1000)				This study (n_e=200)		SAP2000 (n_e=1000)			
	ξ		ξ				ξ		ξ			
	1/5	1/3	1/5	Dif.%	1/3	Dif.%	1/5	1/3	1/5	Dif.%	1/3	Dif.%
1	26.3	44.1	26.4	-0.38	44.5	-0.91	11.8	18.5	11.9	-0.85	18.7	-1.08
2	52.9	78.4	52.9	0.00	78.4	0.00	12.4	19.0	12.4	0.00	19.1	-0.53
3	58.0	79.6	58.4	-0.69	79.8	-0.25	14.8	24.8	14.9	-0.68	25.0	-0.81
4	70.3	106.4	70.4	-0.14	107.0	-0.56	41.3	44.9	41.2	0.24	44.7	0.45
5	83.2	108.2	83.3	-0.12	107.9	0.28	42.1	64.8	-	-	65.2	-0.62
6	96.3	137.9	-	-	137.5	0.29	43.3	70.0	43.6	-0.69	70.2	-0.29

(a=2 mm, R_2=13 mm, R_2/R_1=0.5, Diff. % = (This study-SAP2000)×100/This study)

R_2/R_1=0.5 (assuming R_2=13 mm=constant). The fixed-fixed and fixed-free boundary conditions are employed. For the cruciform cross-section (see Fig. 5(e)), keeping a=2 mm as constant, two different thickness-to-side ratios ξ=1/5, 1/3 are considered, and the computed torsional inertia parameters for these ratios are $\bar{I}_t = 0.00519$ and 0.02313 (see Table 6). The first six natural frequency results are compared using SAP2000 (via Section Designer) in Table 12. In the case of the fixed-fixed boundary condition, with respect to the fundamental natural frequency for the ξ=1/5 ratio, the increase for the ξ=1/3 ratio is 67.7%. Similarly, in the case of the fixed-free boundary condition, with respect to the fundamental natural frequency for the ξ=1/5 ratio, the increase for the ξ=1/3 ratio is 56.8%.

6. Conclusions

The literature on torsion employs the divergence theorem and implements Eq. (9) to calculate the torsional moment of inertia for non-circular cross-sections. This study demonstrates that this type of evaluation is not free from the boundary conditions and requires extra calculations for multiply connected cross-section regions. Alternatively, the proposed formulation procedure is original for the literature and it implements the direct calculation of the torsional rigidity via Eq. (17), which offers a unique method for arbitrarily shaped simply or multiply connected regions. Present formulation is verified with a composite cross-section example and is proven to be successful for several other types of regions. The formulation is suitable and easy to implement with a simple FE. In these analyses, thin-thick closed or open square box and cruciform sections are handled which are all original for the literature. The mixed FE formulation of a helicoidal bar is based on the Timoshenko beam theory, and the documentation of the corresponding functional exists in Omurtag and Aköz (1992). The finite element formulation of the non-cylindrical helix geometry is derived using the exact curvatures at the nodal points and their interpolations through the element axis. The accuracy and range of the proposed torsional moment of the inertia formulation is also verified by the free vibration analysis of cylindrical, conical, barrel and hyperboloidal helicoidal bars under fixed-fixed, fixed-free boundary conditions with the mixed

FEM. The cylindrical helix with equilateral triangular cross-section is solved analytically by Yu and Hao (2011) including the warping of the cross-section and by the results of ANSYS. Although warping is not considered in our formulations, our results are in between these results, which is quite satisfactory with percent errors in the range of 0.29 and 2.53 for the first five modes. Through the analysis, the results are obtained by using 200 curved isoparametric elements of the proposed formulation whereas for SAP2000 the number of elements necessary for an asymptotic convergence is 1000, since they are straight members. The solution of the non-cylindrical helicoidal bars with the noncircular cross-sections (thin-thick close and open square box sections, cruciform) are completely original for the literature and they are benchmark examples. Finally, the convergence of the proposed finite element formulations is fast and reliable.

Acknowledgments

This research is supported by The Scientific and Technological Research Council of Turkey under Project no: 111M308 and it is gratefully acknowledged by the authors.

References

ANSYS (2011), SAS IP, Inc., ANSYS Workbench 2.0 Framework Version 14.0.0 Canonsburg PA. USA.

Arutunan, N.X. and Abraman, B.L. (1963), *Torsion of Elastic Bodies*, State Publisher, Physics-Mathematics Series, Fizmatgiz, Moscow. (in Russian)

Busool, W. and Eisenberger, M. (2002), "Free vibration of helicoidal beams of arbitrary shape and variable cross section", *J. Vib. Acoust.*, **124**, 397-409.

Darılmaz, K., Orakdogen, E., Girgin, K. and Küçükarslan, S. (2007), "Torsional rigidity of arbitrarily shaped composite sections by hybrid finite element approach", *Steel Compos. Struct.*, **7**(3), 241-251.

Eisenberger, M. (1990), "Exact static and dynamic stiffness matrices for general variable cross section members", *AIAA J.*, **28**, 1105-1109.

Ely, J.F. and Zienkiewicz, O.C. (1960), "Torsion of compound bars-A relaxation solution", *Int. J. Mech. Sci.*, **1**, 356-365.

Eratlı, N., Argeso, H., Çalım, F.F., Temel, B. and Omurtag, M.H. (2014), "Dynamic analysis of linear viscoelastic cylindrical and conical helicoidal rods using the mixed FEM", *J. Sound Vib.*, **333**(16), 3671-3690.

Eratlı, N., Ermis, M. and Omurtag, M.H. (2015), "Free vibration analysis of helicoidal bars with thin-walled circular tube cross-section via mixed finite element method", *Sigma J. Eng. Nat. Sci.*, **33**(2), 200-218.

Fard, K.M. (2014), "Higher order free vibration of sandwich curved beams with a functionally graded core", *Struct. Eng. Mech.*, **49**(5), 537-554.

Friedman, Z. and Kosmatka, J.B. (2000), "Torsion and flexure of a prismatic isotropic beam using the boundary element method", *Comput. Struct.*, **74**, 479-494.

Fung, Y.C. (1965), *Foundations of Solid Mechanics*, Prentice-Hall, Englewood Cliffs, New Jersey.

Girgin, K. (2006), "Free vibration analysis of non-cylindrical helices with, variable cross-section by using mixed FEM", *J. Sound Vib.*, **297**, 931-945.

Hermann, L.R. (1965), "Elastic torsional analysis of irregular shapes", *J. Eng. Mech.*, ASCE, **91**(6), 11-19.

Jiang, W., Jones, W.K., Wang, T.L. and Wu, K.H. (1991), "Free vibrations of helical springs", *J. Appl. Mech.*, **58**, 222-228.

Krahula, J.L. and Lauterbach, G.F. (1969), "A finite element solution for Saint-Venant torsion", *AIAA J.*, **7**(12), 2200-2203.

Lamancusa, J.S. and Saravanos, D.A. (1989), "The torsional analysis of bars with hollow square cross-

sections", *Finite Elem. Anal. Des.*, **6**, 71-79.
Lee, J. (2007a), "Free vibration analysis of cylindrical helical springs by the pseudospectral method", *J. Sound Vib.*, **302**, 85-196.
Lee, J. (2007b), "Free vibration analysis of non-cylindrical helical springs by the pseudospectral method", *J. Sound Vib.*, **305**, 543-551.
Li, Z., Ko, J.M. and Ni, Y.Q. (2000), "Torsional rigidity of reinforced concrete bars with arbitrary sectional shape", *Finite Elem. Anal. Des.*, **35**, 349-361.
Lin, Y. and Pisano. A.P. (1987), "General dynamic equations of helical springs with static solution and experimental verification", *J. Appl. Mech*, **54**, 910-917.
Love, A.E.M. (1899), "The propagation of waves of elastic displacement along a helical wire", *Tran. Cambridge Philos. Soc.*, **18**, 364-374.
Michell, J.H. (1890), "The small deformation of curves and surfaces with application to the vibrations of a helix and a circular ring", *Mess. Math.*, **19**, 68-82.
Mottershead, J.E. (1980), "Finite elements for dynamical analysis of helical rods", *Int. J. Mech. Sci.*, **2**(1), 267-283.
Murray, N.W. (1986), *Introduction to the Theory of Thin-Walled Structures*, Clarendon, Oxford.
Nagaya, K., Takeda, S. and Nakata, Y. (1986), "Free vibration of coil springs of arbitrary shape", *Int. J. Numer. Meth. Eng.*, **23**, 1081-1099.
Oden, J.T. and Reddy, J.N. (1976), *Variational Method in Theoretical Mechanics*, Springer-Verlag, Berlin.
Omurtag, M.H. and Aköz, A.Y. (1992), "The mixed finite element solution of helical beams with variable cross-section under arbitrary loading", *Comput. Struct.*, **43**(2), 325-331.
Pearson, D. (1982), "The transfer matrix method for the vibration of compressed helical springs", *J. Mech. Eng. Sci.*, **24**(4), 163-171.
Rajasekaran, S. (2013), "Free vibration of tapered arches made of axially functionally graded materials", *Struct. Eng. Mech.*, **45**(4), 569-594.
Roark, R.J. (1954), *Formulas for Stress and Strain*, McGraw-Hill, New York.
SAP2000 (2013), Computers and Structures, Inc., SAP2000 Ultimate Version 16.0.0 Berkeley CA. USA.
Sapountzakis, E.J. (2001), "Nonuniform torsion of multi-material composite bars by the boundary element method", *Comput. Struct.*, **79**, 2805-2816.
Sapountzakis, E.J. and Mokos, V.G. (2004), "Nonuniform torsion of bars variable cross section", *Comput. Struct.*, **82**, 703-715.
Smith, J. (1996), "Highly Accurate Beam Torsion Solutions Using the p-Version Finite Element Method", National Aeronautics and Space Administration, Langley Research Center.
Timoshenko, S. and Goodier, J.N. (1969), *Theory of Elasticity*, McGraw-Hill, New York.
Tufekci, E. and Yigit, O.O. (2012), "Effects of geometric parameters on in-plane vibrations of two-stepped circular beams", *Struct. Eng. Mech.*, **42**(2), 131-152.
Wang, C.T. (1953), *Applied Elasticity*, McGraw-Hill, New York.
Wittrick, W.H. (1966), "On elastic wave propagation in helical spring", *Int. J. Mech. Sci.*, **8**, 25-47.
Yıldırım, V. (1996), "Investigation of parameters affecting free vibration frequency of helical springs", *Int. J. Numer. Meth. Eng.*, **39**(1), 99-114.
Yıldırım, V. and İnce, N. (1997), "Natural frequencies of helical springs of arbitrary shape", *J. Sound Vib.*, **204**(2), 311-329.
Yıldırım, V. (1997), "Free vibration analysis of non-cylindrical coil springs by combined use of the transfer matrix and complementary functions methods", *Commun. Numer. Meth. Eng.*, **13**, 487-494.
Yıldırım, V. (1998), "A parametric study on the free vibration of non-cylindrical helical springs", *J. Appl. Mech.*, ASME, **65**, 157-163.
Yıldırım, V. (2002), "Expressions for predicting fundamental natural frequencies of non-cylindrical helical springs", *J. Sound Vib.*, **252**(3), 479-491.
Yıldırım, V. (2012), "On the linearized disturbance dynamic equations for buckling and free vibration of cylindrical helical coil springs under combined compression and torsion", *Meccanica*, **47**, 1015-1033.
Yoshimura, Y. and Murata, Y. (1952), "On the elastic waves propagated along coil springs", *Inst. Sci. Tech.*,

Tokyo Univ., **6**(1), 27-35.
Yu, A.M., Yang, C.J. and Nie, G.H. (2010), "Analytical formulation and evaluation for free vibration of naturally curved and twisted beams", *J. Sound Vib.*, **329**, 1376-1389.
Yu, A.M. and Hao, Y. (2011), "Free vibration analysis of cylindrical helical springs with noncircular cross-sections", *J. Sound Vib.*, **330**, 2628-2639.
Yu, A.M. and Hao, Y. (2012), "Improved Riccati transfer matrix method for free vibration of non-cylindrical helical springs including warping", *Shock Vib.*, **19**, 1167-1180.
Yu, A.M. and Hao, Y. (2013a), "Effect of warping on natural frequencies of symmetrical cross-ply laminated composite non-cylindrical helical springs", *Int. J. Mech. Sci.*, **74**, 65-72.
Yu, A.M. and Hao, Y. (2013b), "Warping effect in free vibration analysis of unidirectional composite non-cylindrical helical springs", *Meccanica*, **48**, 2453-2465.
Zhu, L., Zhao, Y. and Wang, G. (2013), "Exact solution for free vibration of curved beams with variable curvature and torsion", *Struct. Eng. Mech.*, **47**(3), 345-359.

CC